Applied Catalysis B: Environmental 253 (2019) 28–40

Contents lists available at ScienceDirect

Applied Catalysis B: Environmental

journal homepage: www.elsevier.com/locate/apcatb

Novel Fenton-like catalyst γ-Cu-Al_2O_3-$Bi_{12}O_{15}Cl_6$ with electron-poor Cu centre and electron-rich Bi centre for enhancement of phenolic compounds degradation and H_2O_2 utilization: The synergistic effects of σ-Cu-ligand, dual-reaction centres and oxygen vacancies

Zhiqun Xie[a], Jiali Zhou[a], Jinnan Wang[a,*], Corvini Philippe François-Xavier[b], Thomas Wintgens[b]

[a] State Key Laboratory of Pollution Control and Resource Reuse & School of the Environment Nanjing University, Nanjing, 210023, China
[b] School of Life Sciences, University of Applied Sciences and Arts Northwestern Switzerland, Basel, 4132, Switzerland

ARTICLE INFO

Keywords:
Electron-poor Cu centre
Selective degradation
Phenolic compounds
σ-Cu-ligand
Oxygen vacancies

ABSTRACT

Novel Fenton-like catalyst γ-Cu-Al_2O_3-$Bi_{12}O_{15}Cl_6$ with electron-poor Cu centre and electron-rich Bi centre was synthesized for selective degradation of phenolic compounds. Different from electron-rich Cu centre catalysts, the electron-poor Cu centre, which was induced by high electronegativity of Bi, could facilitate the formation of σ-Cu-ligand with phenolic compounds. On one hand, H_2O_2 could directly oxidize σ-Cu-ligand to HO-adduct radicals with the generation of ·OH. Meanwhile, Cu(II) in the σ-Cu(II) complexes could be reduced to Cu(I) by oxidization of the HO-adduct radicals to hydroxylation products. Such reaction not only prevented Cu(II) from oxidizing H_2O_2 to $HO_2^{\cdot}/O_2^{\cdot-}$ but also enhanced the redox cycle of Cu(II)/Cu(I), which improved the catalytic activity and H_2O_2 utilization. On the other hand, although the σ-Cu-ligand was gradually decreased with the decrease of phenolic compounds, dual-reaction centre played the dominant role in catalytic reaction. In addition, large amounts of oxygen vacancies (OVs) are formed in $Bi_{12}O_{15}Cl_6$ during the calcining process (BiOCl→ $Bi_{12}O_{15}Cl_6$), which can also increase the generation of OH. Thus, both electron-rich Bi center and OVs could still reduce H_2O_2 to ·OH for organics degradation even without the formation of σ-Cu-ligand. Being attributed to the synergistic effect of σ-Cu-ligand, dual-reaction centre and OVs mentioned above, γ-Cu-Al_2O_3-$Bi_{12}O_{15}Cl_6$ achieved high catalytic activity for phenolic compounds degradation and utilization efficiency of H_2O_2 (η). In addition, various analytic methods (XPS, TPR, FT-IR, Raman, EPR and solid-state EPR) were used to prove the synergistic effect of the electron-poor/rich centre, σ-Cu-ligand and OVs of catalyst.

1. Introduction

Due to formation of σ-Cu-ligand between phenolic −OH groups and surface Cu, lattice doping Cu-based catalysts could selectively degrade phenolic compounds [1]. Different from classic Fenton reaction mechanism, H_2O_2 could directly attack σ-Cu-ligand with the generation of •OH and HO-adduct radicals. Notably, Cu(II) in the σ-Cu(II) complexes could be reduced to Cu(I) by oxidation of HO-adduct radicals to hydroxylation products, which not only prevented Cu(II) from oxidizing H_2O_2 to $HO_2^{\cdot}/O_2^{\cdot-}$ but also promoted the redox cycle of Cu(II)/Cu(I) [2]. Thus, σ-Cu-ligand played important role in selective degradation of phenolic compounds and utilization of H_2O_2. However, with the degradation of phenolic compounds in the reaction system, the formation of σ-Cu-ligand would be obviously decreased, which made the organics degradation process follow the classic Fenton reaction mechanism (Eqs. (1) and (2)). Thus, the problems of rate limitation step (Eq. (1)) and low H_2O_2 utilization in classic Fenton reaction still remaine d to be resolved.

$$Cu\ (I) + H_2O_2 = Cu(II) + OH^{\cdot} + OH^{-}\ (k = 4.6 \times 10^2\ M^{-1}\ s^{-1}) \quad (1)$$

$$Cu\ (II) + H_2O_2 = Cu(I) + HO_2^{\cdot} + H^{+}\ (k = 1.0 \times 10^4\ M^{-1}\ s^{-1}) \quad (2)$$

On the other hand, in order to resolve the problems of classic Fenton reaction, Cu-based catalysts with dual-reaction centres were constructed to enhance the catalytic activity and selective conversion H_2O_2 to ·OH [3]. By doping of different electro-negative metals, the non-uniform distribution of electrons density of lattice oxygen is formed, which induced the formation of electron-rich centre and electron-poor centre. Since organics and H_2O_2 were respectively accumulated around the electron-poor centre and electron-rich centre, this galvanic-like cell

* Corresponding author.
E-mail address: wjnnju@163.com (J. Wang).

https://doi.org/10.1016/j.apcatb.2019.04.032
Received 16 January 2019; Received in revised form 9 April 2019; Accepted 11 April 2019
Available online 16 April 2019
0926-3373/

effect could realize the highly selective reduction of H_2O_2 and oxidation of organics. Previous literature had already reported that Fenton-like catalyst (OHCCN/CuCo-Al_2O_3) with electron-rich Cu centre could offer two electron transfer routes for generation of ·OH [4]: one was from the electron-rich Cu centre to H_2O_2 and the other was from H_2O to the N atom of OH − CCN. Our previous studies also demonstrated that introduction of g–C_3N_4 and C − dots into γ-Cu-Al_2O_3 could induce the formation of electron-rich Cu centre and electron-deficient π-electron conjugated system, which could simultaneously enhance the catalytic activity and H_2O_2 utilization [5]. However, electron-rich Cu centre catalysts could not form σ-Cu-ligand with phenolic compounds because organics were preferentially accumulated around the electron-poor centre, which leaded to a low mineralization rate of phenolic compounds [5,6]. Thus, it is expected to construct electron-poor Cu centre catalyst by introduction of higher electronegative metal into Cu-Al_2O_3, which can not only possess dual-reaction centre effect but also facilitate the formation of σ-Cu-ligand with phenolic compounds, resulting in enhancement of H_2O_2 utilization and selective degradation of phenolic compounds.

Compared with Cu (1.9 eV), Bi (2.02 eV) has higher electronegativity. Various Bi oxidants were investigated as photocatalysts and Fenton-like catalysts with the case of $BiVO_4$ [7–11], Bi_2O_3 [12,13], and BiOI [14–17]. Among them, Bismuth oxychloride (BiOCl) is a V − VI − VII ternary, p-type semiconductor with many attractive properties which due to its unique, layered atomic structure, possessing an internal static electric field perpendicular to each layer [8,18,19]. Previous literatures also reported that BiOCl modified with Cu could reduce the photo-carriers recombination, which suggested the improvement of the inner charge transfer rate [20,21]. Furthermore, by calcination of BiOCl, the product ($Bi_{12}O_{15}Cl_6$) with lower activation energy, could achieve better electrical conduction and higher photoconductivity [22,23]. Thus, introduction of $Bi_{12}O_{15}Cl_6$ into Cu-Al_2O_3 might induce the formation of electron-poor Cu centre and electron-rich Bi centre, which can selectively degrade phenolic compounds by the synergistic effect of σ-Cu-ligand and dual-reaction centres. In addition, oxygen vacancies (OVs), which are formed during the calcination process of BiOCl to $Bi_{12}O_{15}Cl_6$, can directly reduce H_2O_2 to ·OH, resulting in enhancement of catalytic activity and H_2O_2 utilization.

Based on the above research background and consumption, novel Fenton-like catalyst γ-Cu-Al_2O_3-$Bi_{12}O_{15}Cl_6$ with electron-poor Cu centre and electron-rich Bi centre was constructed for selective catalytic degradation of phenolic compounds. Different from traditional electron-rich Cu center catalysts, introduction of $Bi_{12}O_{15}Cl_6$ into γ-Cu-Al_2O_3 will induce the formation of electron-poor Cu centre which can facilitate the formation of σ-Cu-ligand with phenolic compounds. During the initial reaction period, σ-Cu-ligand play dominant role in mineralization of phenolic compounds and utilization of H_2O_2. H_2O_2 could directly oxidize σ-Cu-ligand with the generation of OH and HO-adduct radicals. Meanwhile, Cu(II) in the σ-Cu-ligand could be reduced to Cu(I) by oxidization of the HO-adduct radicals to hydroxylation products. Such process not only prevented Cu(II) from oxidizing H_2O_2 to $HO_2^{\cdot}$/$O_2^{\cdot}$ − but also promoted the redox cycle of Cu(II)/Cu(I). On the other hand, with the decrease of σ-Cu-ligand, dual-reaction centres gradually play the dominant role in selective H_2O_2 conversion to OH and organics degradation. In addition, OVs on the surface of γ-Cu-Al_2O_3-$Bi_{12}O_{15}Cl_6$ can reduce H_2O_2 to OH, which also enhance the catalytic activity and H_2O_2 utilization.

2. Experimental

2.1. Chemicals

Glucose ($C_6H_{12}O_6$), copper(II) Chloride dihydrate ($CuCl_2{\cdot}2H_2O$), Potassium Phosphate Monobasic(KH_2PO_4), hydrogen peroxide (H_2O_2, 30%w/w), ammonia and citric acid were purchased from the National Medicines Corporation Ltd. of China. Horseradish peroxidas(POD), Rhodamine B (Rh B), Bisphenol A (BPA), 2-Chlorophen-ol, aluminium isopropoxide [$Al(OiPr)_3$], Bismuth nitrate pentahydrate ($Bi(NO3)_3{\cdot}5H_2O$), 2,2′-azino-bis (3-ethylbenzothiazoline-6-sulfonate) (ABTS) and 5,5-Dimethyl-1-pyrroline N-oxide (DMPO) were supplied by Aladdin Industrial Corporation, China. Deionized water was used in this study. All chemicals were A. R. grade (> 99%) and were used without further purification.

2.2. Preparation of catalysts

γ-Cu-Al_2O_3-$Bi_{12}O_{15}Cl_6$ was prepared by a modified evaporation-induced self-assembly reaction as follows. Typically, 0.64 g Bismuth nitrate pentahydrate was dissolved in 5 mL nitric acid solution (2 M), and the solution was diluted to 100 ml using deionized water. Then 0.3 g citric acid was dissolved in this solution with adjustment of pH to 6.5 by using ammonia. 8.4 g of $Al(OiPr)_3$, 0.4 g of $CuCl_2{\cdot}2H_2O$, and 7.2 g of glucose were added in solution under stirring at 40 °C for 12 h. For removal of water and other volatiles, the mixture was evaporated at 100 °C with mechanical stirring. Then the mixture was calcined in a muffle furnace at 600 °C for 6 h to obtain the product (γ-Cu-Al_2O_3-$Bi_{12}O_{15}Cl_6$). After washed with deionized water for several times, the catalyst was dried at 80 °C for 6 h.

To optimize the doping content of $Bi_{12}O_{15}Cl_6$, γ-Cu-Al_2O_3-$Bi_{12}O_{15}Cl_6$ composites with different Bi contents were prepared in the present work. According to the adding amount of $Bi(NO_3)_3{\cdot}5H_2O$ during preparation process, γ-Cu-Al_2O_3-$Bi_{12}O_{15}Cl_6$ composites synthesized with different Bi content were named as 0.32CAB, 0.64CAB, 1.28CAB and 2.64CAB. In addition, γ-Cu-Al_2O_3, BiOCl, $Bi_{12}O_{15}Cl_6$ and Al_2O_3 were also prepared for comparative studies.

2.3. Characterization of catalysts and catalytic mechanism

Surface morphology and lattice fringe of γ-Cu-Al_2O_3-$Bi_{12}O_{15}Cl_6$ were characterized by field emission scanning electron microscopy (FESEM, QUANTA FEG 250) and transmission electron microscopy (TEM, JEM-200CX), respectively. X ray fluorescence spectrometer (XRF, ARL-9800) was used to analyze the doping amount of Cu and Bi in the samples. To observe the crystal structure of the catalysts, X-ray diffraction (XRD) spectra were collected using a XRD-6000 X-ray diffractometer (Shimadzu, Japan) with a Cu K radiation (= 1.5406 Å) over the 2θ range of 10–60°. Gas sorption analyzer (NOVA2000e) was used to measure BET surface area and pore structure of catalysts. The UV − vis diffuse reflectance spectroscopy (UV − vis DRS) of γ-Cu-Al_2O_3-$Bi_{12}O_{15}Cl_6$ was measured by UV-2600 spectrophotometer (SHIMADZU, Japan), which could confirm whether Cu was successfully doped into crystal lattice of γ-Al_2O_3. To further study the valence state and chemical bond of catalysts, X-ray photoelectron spectroscopy (XPS) of samples were analyzed by a PHI 5000 Versa Probe instrument using monochromatic Al Kα radiation (225 W, 15 mA, 15 kV). During the deconvolution process of XPS curves; all binding energies were referenced to the C 1 s peak at 284.8 eV. In addition, EPR spectra of the solid samples were obtained using the EMX-10/12 electron paramagnetic resonance spectrometer, which could provide useful information of the electronic structure of paramagnetic Cu (II). Meanwhile, it could be also used to confirm the existence of OVs on catalysts.

Notably, in order to clearly illustrate the different catalytic mechanism of γ-Cu-Al_2O_3-$Bi_{12}O_{15}Cl_6$ from traditional electron-rich centre (Cu) catalysts and classic Fenton reaction, Temperature-programmed reduction (TPR-H_2), FT-IR, in situ Raman and DMPO-trapped EPR spectra were deeply analyzed. TPR-H_2 experiments of catalysts were conducted using a Micromeritics Auto Chem II 2920 instrument for characterization of the redox properties of dual-reaction centres (Cu, Bi). FT-IR spectra of catalysts were used to confirm the formation of σ-Cu-ligand between electron-poor Cu centre and phnolic compounds. In situ Raman spectra of suspension (γ-Cu-Al_2O_3-$Bi_{12}O_{15}Cl_6$ + H_2O_2) in the absence and presence of BPA at different reaction time are conducted to

demonstrate the different catalytic mechanism from traditional electron-rich centre (Cu) catalysts. To confirm the main active species, DMPO-trapped EPR signals were detected in different air saturated methanol/aqueous dispersions of the corresponding catalysts in the absence and presence of H_2O_2 and BPA. In addition, to evaluate the electron transfer ability in Fenton-like system, electrochemical measurements were conducted by the electrochemical workstation (CHI660E, Shanghai, China) with a conventional three-electrode system (100 mL 0.5 M Na_2SO_4 containing 0.01 mM H_2O_2 as the electrolyte). Time-resolved lifetime curve was performed using a HORIBA JOBIN YVON FL-TCSPC fluorescence spectrometer. The probe beam was a 370 nm laser beam (with a repetition frequency of 1 MHz).

2.4. Catalytic performance

The catalytic activities of catalysts were evaluated by degradation of phenolic compounds (BPA, 2-Chlorophenol) and non-phenolic compound (Rh B). Typically, 100 mL aqueous solutions with certain organic and catalyst were mixed in 150 mL beaker flasks. After magnetically stirred for 30 min, 8 mM H_2O_2 was added in the suspensions with magnetic stirring (120 rpm). During the catalytic degradation process, 1 mL aliquots were sampled at given time intervals, and then filtered through a Millipore filter (0.45 μm) prior to the analysis. The residual concentrations of BPA and 2-Chlorophenol in solution were measured by 1200 series HPLC equipped with a UV detector. The residual concentration of Rh B in solution was determined by UV-1800 UV–vis spectrometer (Shimadzu, Japan). Furthermore, five successive cycles catalytic degradation of BPA and Rh B were carried out to test the catalyst stability. The leaching of metallic ions (Cu, Al and Bi) in suspensions after successive catalytic degradation was measured by ICE3500 atomic absorption spectrometer (Thermo ScientificM).

In addition, the utilization efficiency of H_2O_2 (η) is defined as the ratio of the stoichiometric H_2O_2 consumption ($[\Delta H_2O_2]_S$) for the mineralization of pollutants to the actual H_2O_2 consumption ($[\Delta H_2O_2]_A$) in the Fenton reaction. The H_2O_2 concentration was determined according to the ABTS method reported in previous work (Supplementary material) [24].

3. Results and discussion

3.1. Morphology and structure of catalysts

γ-Cu-Al_2O_3-$Bi_{12}O_{15}Cl_6$ shows cotton-like amorphous structure (Fig. 1A), which is due to the generation of $BiCl_3$ stream [15BiOCl (s) → 3$BiCl_3$ (g) + $Bi_{12}O_{15}Cl_6$ (s)] (Fig. S1) during the calcining process (temperature > 400°C) [22]. Such cotton-like amorphous structure might provide more active sites for catalytic reaction. Furthermore, doping of $Bi_{12}O_{15}Cl_6$ improved the exposure of copper on catalyst surface rather than in the bulk matrix. According to the XPS and X ray fluorescence spectrometer results (Table S1), copper on the surface of γ-Cu-Al_2O_3-$Bi_{12}O_{15}Cl_6$(2.64CAB) increased from 1.05 to 1.32 (wt%) compared with γ-Cu-Al_2O_3. Thus, Al, Cu, O, Bi and Cl are homogenously distributed on catalyst surface (Fig. 1B). In addition, $Bi_{12}O_{15}Cl_6$ nano-particles are adhered to the surface of γ-Cu-Al_2O_3, which construct the heterostructure (Fig. 1C). Notably, HRTEM image (Fig. 1D) clearly shows that copper is perfectly embedded in the lattice of γ-Al_2O_3. The lattice fringe with the interplanar spacing of 0.21 nm is corresponded to the (111) plane of Cu, while cloud-like materials without lattice fringe is amorphous structured γ-Al_2O_3. Moreover, the absorption band at 750 nm in the UV − vis DRS of γ-Cu-Al_2O_3-$Bi_{12}O_{15}Cl_6$ (Fig. S2) is assigned to the electron transitions in Cu(II) in octahedral sites of the spinel lattice [25], which also confirms the incorporation of Cu to γ-Al_2O_3 during the preparation process of γ-Cu-Al_2O_3-$Bi_{12}O_{15}Cl_6$. In addition, the N_2 adsorption/desorption isotherms of γ-Cu-Al_2O_3-$Bi_{12}O_{15}Cl_6$ is in accord with typical IV isotherms with the H3 hysteresis loop (Fig. S3), suggesting the aggregation of slit-shaped pores and the meso-pore structure of catalysts [26]. With the increase of $Bi_{12}O_{15}Cl_6$ content, the pore volume of γ-Cu-Al_2O_3-$Bi_{12}O_{15}Cl_6$ gradually decreases, which indicates that $Bi_{12}O_{15}Cl_6$ are uniformly doped on the surface and into interior of catalysts.

The strong diffraction peaks near 1° in low-angle XRD patterns (Fig. S4 A) are ascribed to the typical pattern of porous structure, which was in agreement with the HRTEM images (Fig. 1D). However, due to the uniform distribution of copper species in γ-Al_2O_3 framework, diffraction peaks corresponding to copper are not observed in the wide angle XRD patterns (Fig. S4BII,III). After doping of $Bi_{12}O_{15}Cl_6$ (Fig. S4BIII), new peaks appear and most of them correspond to $Bi_{12}O_{15}Cl_6$ (JCPDS card No. 70 − 0249). The strongest diffraction peak at 2θ = 30.12° is ascribed to the (413) planes of $Bi_{12}O_{15}Cl_6$, suggesting the preferential orientation of (413) planes [27].

XPS spectra were used to further analyze atomic valence state and chemical bond of the catalysts surface. The peak at 74.2 eV is assigned to Al − O–Al of pure γ-Al_2O_3 (inset image of Fig. S5 A). Two binding energies (BEs) for Al^{3+} located at 74.2 and 75.3 eV in the spectra of γ-Cu-Al_2O_3-$Bi_{12}O_{15}Cl_6$(0.64CAB), are assigned to Al − O–Al and Al − O–Cu, respectively (Fig. S5-A). Furthermore, peaks at 932.7 eV, 934.0 eV and 942.4 eV are corresponded to the reduction state, oxidation state and fluctuation peaks of the copper species, respectively. Notably, Auger kinetic energy at 574.7 eV further confirms the existence of Cu(I) rather than Cu° (Fig. 2B), which also confirm the lattice doping of Cu in γ- Al_2O_3. Since the atomic radius of Cu is bigger than Al, lattice doping of Cu into γ-Al_2O_3 will make the characteristic peak of Al shift to low-angle region. The local magnification image (Fig. S4 C) can clearly show that the characteristic peak of γ-Al_2O_3 shift from 67.06° to 66.85° (γ-Cu-Al_2O_3) and 66.64° (γ-Cu-Al_2O_3-$Bi_{12}O_{15}Cl_6$), which can further confirm the lattice doping of Cu into γ-Al_2O_3. In addition, more obvious shift of characteristic peak (γ-Al_2O_3) of γ-Cu-Al_2O_3-$Bi_{12}O_{15}Cl_6$ suggests that $Bi_{12}O_{15}Cl_6$ contributes to the lattice doping of Cu into γ-Al_2O_3.

In addition, the XPS curve fittings indicate that atomic ratio of Cu (II) to Cu (I) is significantly increased from 1:1 to 1.2:1 and 1.43:1 as the Bi content increases from 0 wt% (γ-Cu-Al_2O_3) to 12.5 wt% (0.64CAB) and 41.2 wt% (2.64CAB), respectively. Thus, doping of $Bi_{12}O_{15}Cl_6$ onto γ-Cu-Al_2O_3 greatly decreased the proportion of Cu(I) on the surface of catalysts. Moreover, peaks of Cu 2p (932.4 eV and 934.0 eV for γ-Cu-Al_2O_3) shift to high binding energy (932.8 eV and 935.2 eV for 2.64CAB) (Fig. 2A–C), which indicates that the strong electronegative Bi significantly decreases the electron density around the Cu center, inducing the formation of electron-poor Cu centre.

In addition, characteristic peaks of Bi $4f_{7/2}$ (158.8 eV) and Bi $4f_{5/2}$ (164.0 eV) are assigned to Bi^{3+} of BiOCl (Fig. 2D). After calcination of pure BiOCl for 6 h at 600 °C, red-shifts of characteristic peaks [Bi $4f_{7/2}$ (159.1 eV) and Bi $4f_{5/2}$ (164.5 eV)] were observed due to the formation of $Bi_{12}O_{15}Cl_6$. However, doping of $Bi_{12}O_{15}Cl_6$ into γ-Cu − Al_2O_3 leads to a blue-shift of the characteristic peaks [Bi $4f_{7/2}$ (158.3 eV) and Bi $4f_{5/2}$ (163.7 eV)], which demonstrate the formation of electron-rich Bi centre and electron-poor Cu centre in γ-Cu-Al_2O_3-$Bi_{12}O_{15}Cl_6$. Notably, OVs can be formed during the calcination process of BiOCl to $Bi_{12}O_{15}Cl_6$, and the localized electrons on OVs are transferred to Bi^{3+} with the generation of lower charge Bi ions ($Bi^{(3-x)+}$) [28,29]. Thus, new peaks with lower binding energy (157.3 eV, 162.7 eV) appear in the spectrum of Bi 4f of γ-Cu-Al_2O_3-$Bi_{12}O_{15}Cl_6$(0.64CAB) (Fig.2E). Moreover, three characteristic peaks of O 1 s in Fig. S5(B) respectively represent the lattice oxygen of $Bi_{12}O_{15}Cl_6$ (OL, 529.6 eV), lattice oxygen of γ − Al_2O_3 (OL, 530.7 eV), and surface hydroxyl oxygen (O − OH, 531.8 eV) which are produced by the reaction between OVs and H_2O. On the contrary, only one O 1 s peak is observed in γ-Cu − Al_2O_3 spectra, indicating the lattice oxygen of γ − Al_2O_3 (OL, 530.9 eV). Thus, XPS spectra suggested the formation of OVs, electron-rich centre (Bi) and electron-poor centre (Cu) in γ-Cu-Al_2O_3-$Bi_{12}O_{15}Cl_6$.

To get a deep insight into the electronic structure of paramagnetic Cu (II), solid electron paramagnetic resonance (EPR) spectra of γ-Cu-

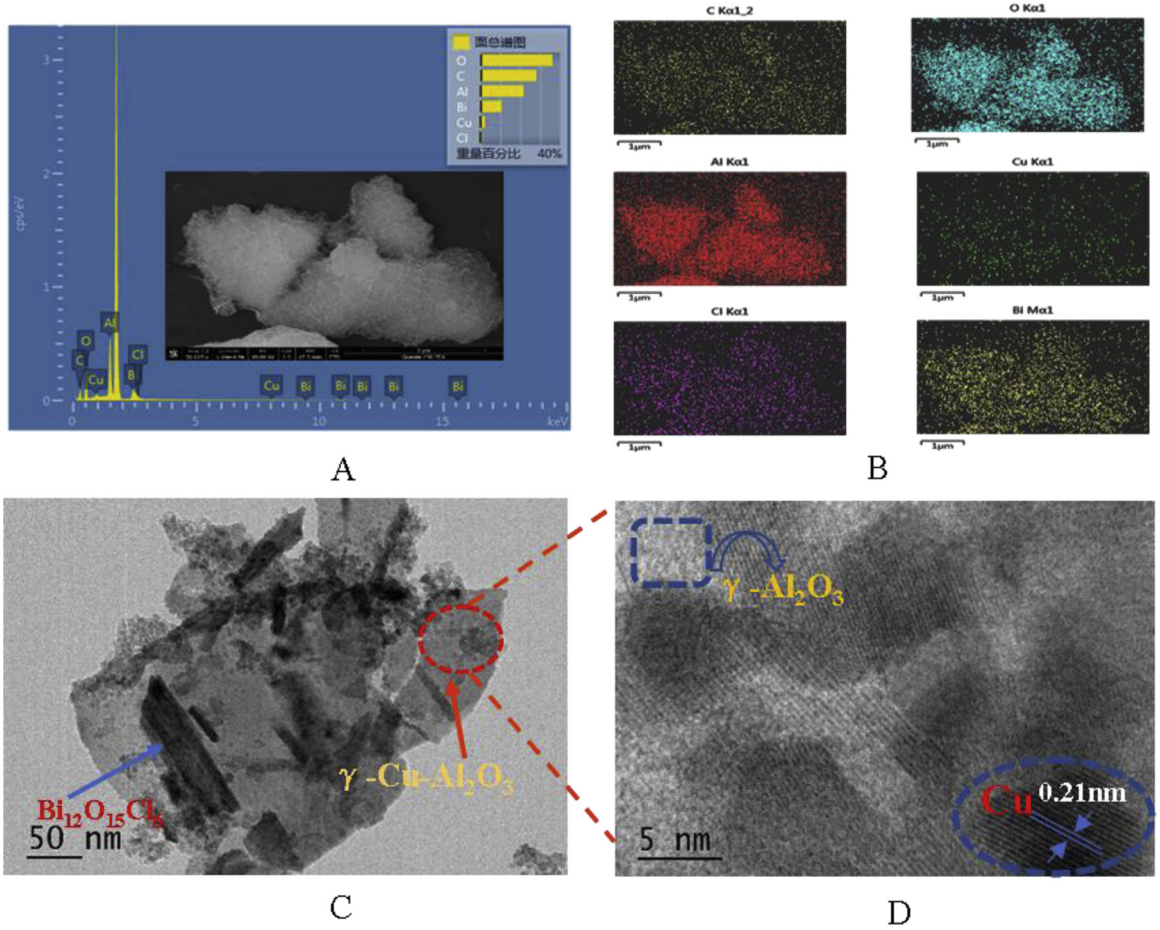

Fig. 1. (A) SEM image of 0.64CAB; (B) EDS element distribution of C, O, Al, Cu, Cl and Bi; (C) TEM image of γ-Cu-Al_2O_3-$Bi_{12}O_{15}Cl_6$(0.64CAB); (D) HRTEM image of γ-Cu-Al_2O_3-$Bi_{12}O_{15}Cl_6$(0.64CAB).

Al_2O_3-$Bi_{12}O_{15}Cl_6$ with different Bi content are analyzed (Fig. 3A). EPR signals with the hyperfine coupling of different samples are clearly observed, suggesting the presence of Cu (II) with I (nuclear spin) = 3/2 (room temperature) (Fig. 3B). The g-tensors of all the samples follow the order of $g_{//} > g_{\perp} > 2.0023(g_e)$ (Table S2), which indicate that the unpaired electron is localized in the dx2-y2 orbital of Cu(II) [30]. Thus, signal shape and the g-tensors demonstrate the six-coordinated Cu (II) with an octahedral geometry structure [30]. In addition, the intensity of the EPR signal could show the Cu (II) content and the single electrons density around the Cu (II). The decrease of peak intensity from 0.64CAB to 2.64CAB is more obvious than that from γ-Cu-Al_2O_3 to 0.64CAB, while the decrease of Cu content from 0.64CAB (4.7%) to 2.64CAB (3.6%) is much lower than that from γ-Cu-Al_2O_3 (6.7%) to 0.64CAB (4.7%). Thus, the decrease of EPR peak intensity of Cu is mainly due to the electron density decrease, which further confirms the formation of electro-poor Cu centre.

The redox properties of catalysts can be characterized by H_2-TPR. There are two characteristic reduction peaks in TPR spectra of γ- Cu-Al_2O_3 (Fig.3C). The peak at 219 °C is ascribed to the lattice doped Cu (II)/Cu(I) which can be easily reduced to Cu° at lower temperature by H_2, while the peak at 246 °C is assigned to CuO particles. As for γ-Cu-Al_2O_3-$Bi_{12}O_{15}Cl_6$, characteristic peaks of CuO almost disappeared, which suggested that all copper was well embedded and dispersed into the lattice of γ-Al_2O_3, which is in accordance with XRD results (Fig. S4C). Thus, the lattice fringe (0.21 nm) corresponded to (111) plane of Cu is clearly observed in amorphous structured γ-Al_2O_3 (Fig. 1D). Notably, the characteristic peak of Cu(II)/Cu(I) obviously shifts to a lower temperature with the increase of Bi content from 0 (γ-Cu-Al_2O_3) to 41.2 wt%(2.64CAB). Such phenomenon could be explained as follows: (1) in γ-Cu-Al_2O_3-$Bi_{12}O_{15}Cl_6$ composite, lattice doped Cu(II)/Cu(I) was well dispersed in the amorphous structured γ-Al_2O_3, which was beneficial for their reduction to Cu°; (2) doping of strong electronegative Bi in γ-Cu-Al_2O_3 induced the formation of electro-poor Cu centre, which also facilitated the reduction of Cu(II)/Cu(I) to Cu°. In addition, the peak at 360 °C of pure $Bi_{12}O_{15}Cl_6$ was assigned to the reduction of Bi (III). After doping of γ-Cu-Al_2O_3, the reduction temperature of Bi(III) to Bi° decreased obviously. On one hand, doping of γ-Cu-Al_2O_3 into $Bi_{12}O_{15}Cl_6$ could increase the dispersion degree of Bi and Cu in catalysts, which was beneficial for their reduction to Bi°. On the other hand, OVs in γ-Cu-Al_2O_3-$Bi_{12}O_{15}Cl_6$ increased with the $Bi_{12}O_{15}Cl_6$ content, which might weaken the Bi-O bond in the γ-Cu-Al_2O_3-$Bi_{12}O_{15}Cl_6$ due to vacancy compensation mechanism [31]. Thus, the reduction temperature of Cu(II)/Cu(I) and Bi(III) decreased after $Bi_{12}O_{15}Cl_6$ was doped in γ-Cu-Al_2O_3. However, as the Bi content was further increased to 52.1% (3.28CAB), the peak of Cu(II)/Cu(I) shifted to the high temperature. This was because excessive $Bi_{12}O_{15}Cl_6$ might cover the Cu(II)/Cu(I), which showed adverse effect on reduction of Cu(II)/Cu(I). Thus, γ-Cu-Al_2O_3-$Bi_{12}O_{15}Cl_6$(2.64CAB) showed the lowest reduction temperature of Cu(II)/Cu(I). In addition, electrochemical impedance spectroscopy (EIS) is used to further evaluate the electron transfer in Fenton like system (Fig. S6). The Nyquist plot diameter follows the order of $\gamma-Al_2O_3$ > γ-Cu − Al_2O_3 > γ-Cu-Al_2O_3-$Bi_{12}O_{15}Cl_6$(0.64CAB) > γ-Cu-Al_2O_3-$Bi_{12}O_{15}Cl_6$(2.64CAB), which indicate that doping of Bi can improve the electron transfer rate of Fenton like system (Fig. 3D). In addition, the carriers life time of samples follow the order of γ-Cu-Al_2O_3 (1.376 ns) < γ-Cu-Al_2O_3-$Bi_{12}O_{15}Cl_6$ (0.64CAB) (1.668 ns) < γ-Cu-Al_2O_3-$Bi_{12}O_{15}Cl_6$ (2.64CAB) (1.894 ns) (Fig. 3E), which are in accordance with the results of UV–vis spectra (Fig. S2) and EIS (Fig. 3D).

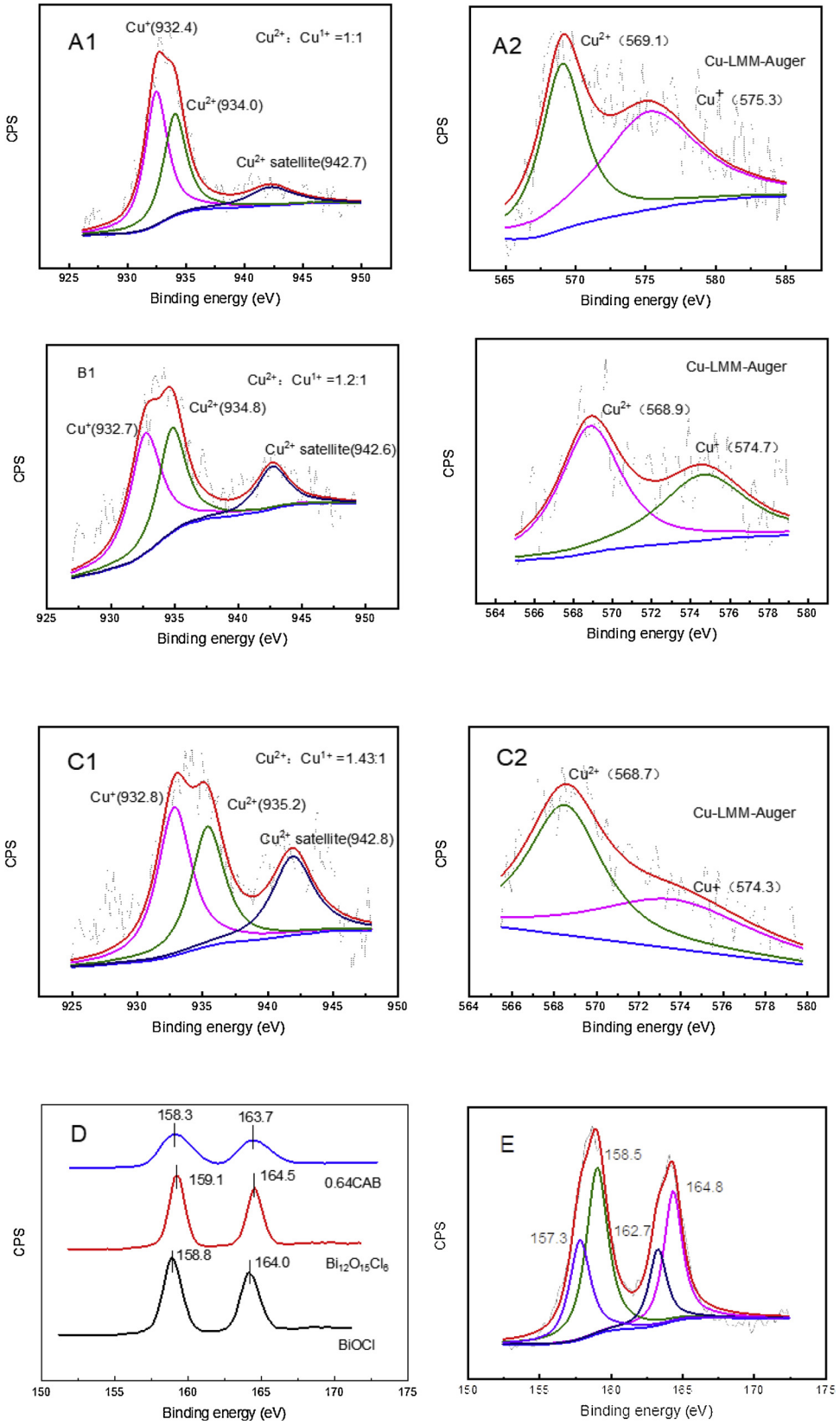

Fig. 2. XPS spectra of Cu 2p for (A-1) γ-Cu-Al_2O_3, (B-1) γ-Cu-Al_2O_3-$Bi_{12}O_{15}Cl_6$(0.64CAB), and (C-1) γ-Cu-Al_2O_3-$Bi_{12}O_{15}Cl_6$(2.64CAB). LMM X-ray induced Auger kinetic energy for (A-2) γ-Cu-Al_2O_3, (B-2) γ-Cu-Al_2O_3-$Bi_{12}O_{15}Cl_6$(0.64CAB), and (C-2) γ-Cu-Al_2O_3-$Bi_{12}O_{15}Cl_6$(2.64CAB). (D) The XPS spectra of Bi 4f of BiOCl, $Bi_{12}O_{15}Cl_6$ and γ-Cu-Al_2O_3-$Bi_{12}O_{15}Cl_6$(0.64CAB). (E) The XPS curve fittings spectra of Bi 4f in γ-Cu-Al_2O_3-$Bi_{12}O_{15}Cl_6$ (0.64CAB).

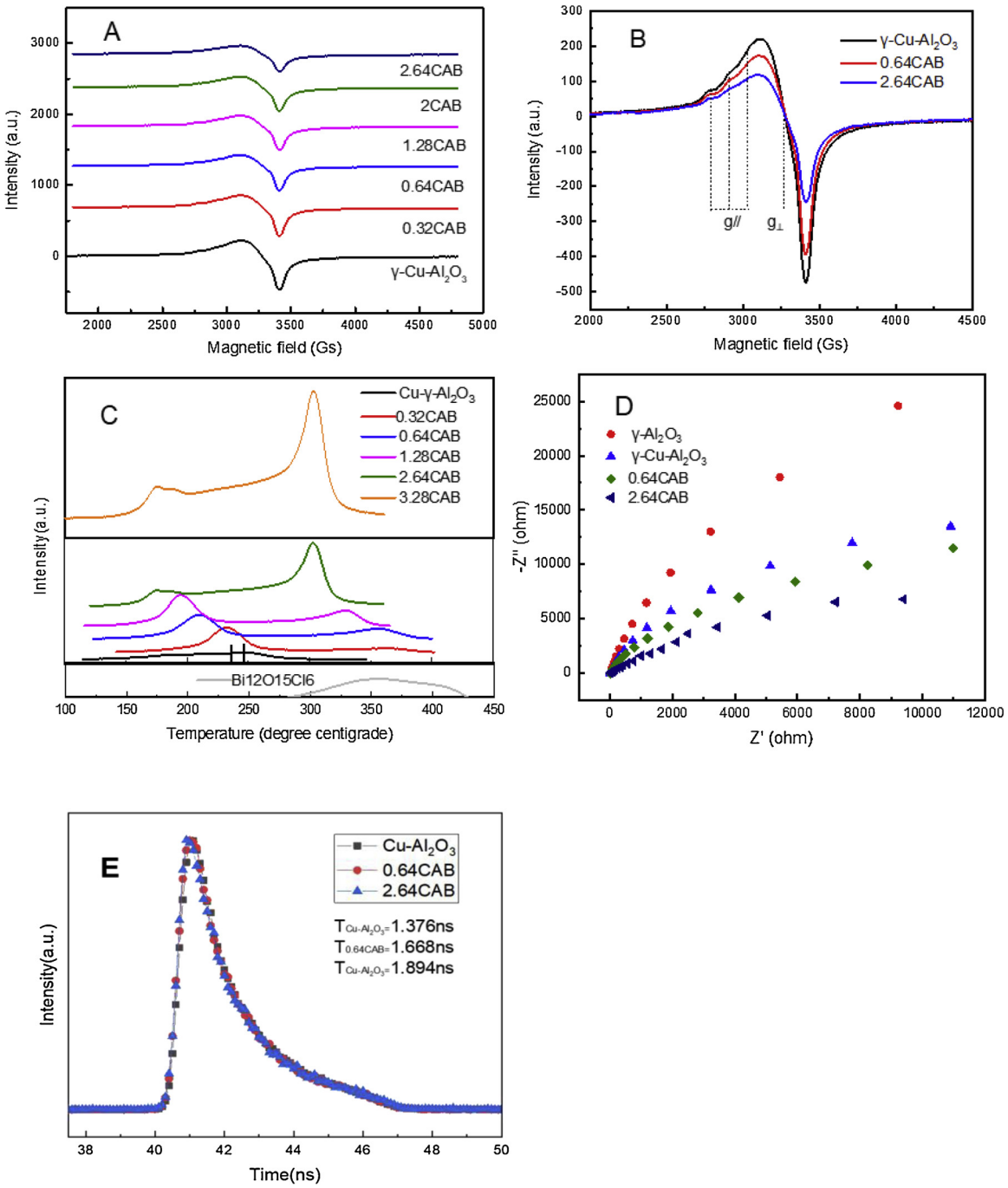

Fig. 3. (A) Solid EPR spectra of γ- Cu-Al_2O_3, 0.32CAB, 0.64CAB, 1.28CAB, 2CAB and 2.64CAB. (B) Enlargement of solid EPR spectra of γ- Cu-Al_2O_3, 0.64CAB and 2.64CAB; (C) TPR profile of $Bi_{12}O_{15}Cl_6$, γ-cu-Al_2O_3, 0.32CAB, 0.64CAB, 1.28CAB and 2.64CAB; (D) EIS of γ-Al_2O_3, γ-Cu-Al_2O_3, 0.64CAB and 2.64CAB with H_2O_2; (E) Time-resolved fluorescence decay spectra of Cu-Al_2O_3, 0.64CAB and 2.64CAB.

Previous literatures have demonstrated that increase of life time of carrier could enhance the charge separation and transfer of catalyst, resulting in the improvement of the catalysis performance [32–36]. Thus, the electron transfer of Fenton like system was improved by doping of $Bi_{12}O_{15}Cl_6$ into γ-Cu-Al_2O_3.

3.2. Catalytic performance

Catalytic degradation of BPA, 2-Chlorophenol and Rh B were used to evaluate the catalytic activities of catalysts. γ-Cu-Al_2O_3-$Bi_{12}O_{15}Cl_6$(0.64CAB) shows the highest catalytic activity for degradation of BPA (Fig. 4A), while γ-Cu-Al_2O_3-$Bi_{12}O_{15}Cl_6$ (2.64CAB) achieves the highest degradation rate of Rh B (Fig. 4B). Such different degradation performance between BPA and Rh B suggested different catalytic mechanisms. Although both σ-Cu-ligand and dual-reaction centres are important for BPA degradation, σ-Cu-ligand plays dominant role in degradation of BPA at the initial reaction period. Since the formation of σ-Cu-ligand relied on the Cu content of catalyst, increase of Bi content decreased the formation of σ-Cu-ligand between BPA and γ-Cu-Al_2O_3-$Bi_{12}O_{15}Cl_6$. However, decrease of Bi content would weaken the dual-reaction centres because of lowering of polarization difference. Thus, γ-Cu-Al_2O_3-$Bi_{12}O_{15}Cl_6$(0.64CAB) shows the highest catalytic activity for degradation of BPA. The similar result was also observed during the catalytic degradation process of 2-Chlorophenol (Fig. S8B).

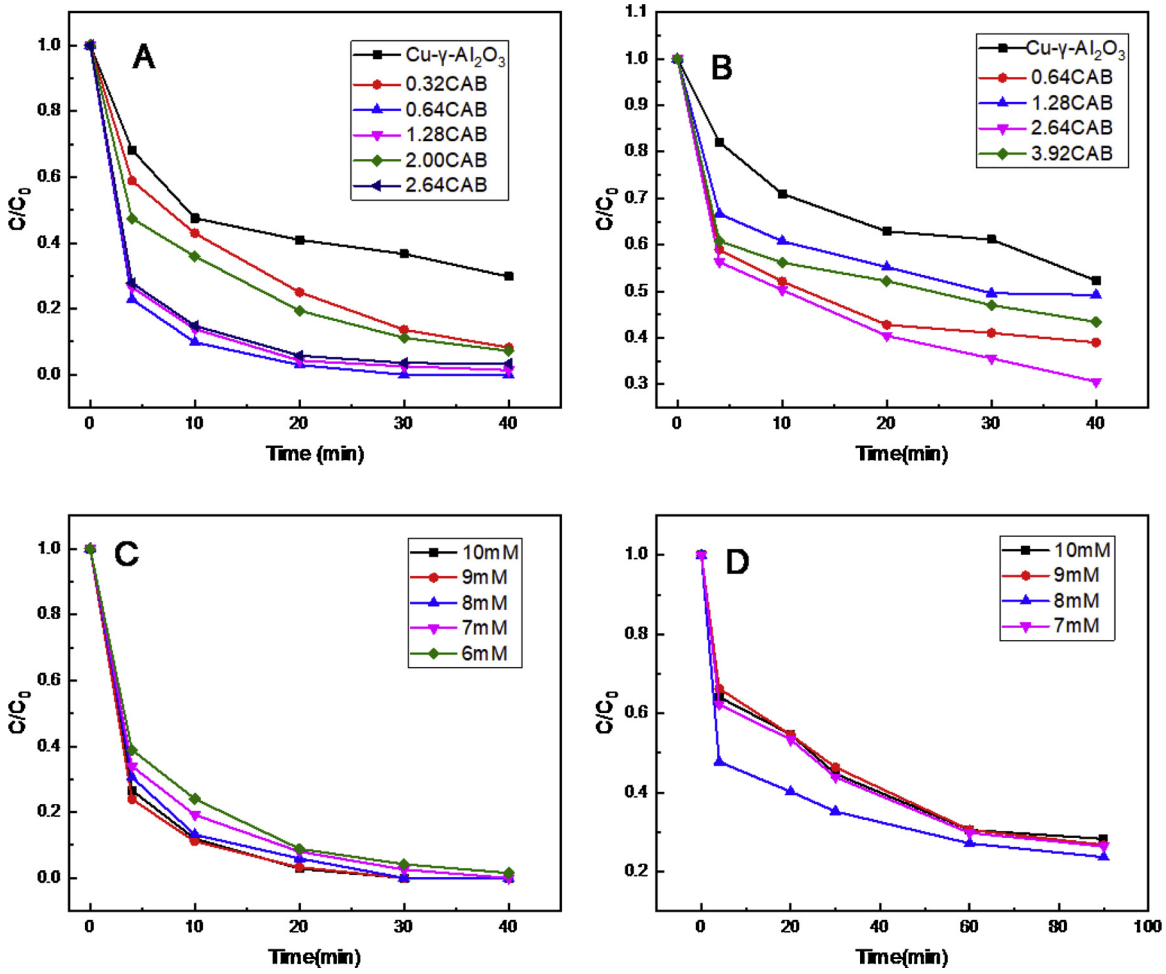

Fig. 4. (A) Degradation of BPA (20 mg/L) over catalysts with different Bi content; (B) Degradation of Rh B ((initial concentration : 10 mg/L) over catalysts with different Bi content; (C) Effect of H_2O_2 dosage on BPA (initial concentration: 20 mg/L) degradation over γ-Cu-Al_2O_3-$Bi_{12}O_{15}Cl_6$(0.64 CAB) (1.0 g /L); (D) Effect of H_2O_2 dosage on TOC removal of BPA ((initial concentration : 20 mg/L) over γ-Cu-Al_2O_3-$Bi_{12}O_{15}Cl_6$(0.64 CAB) (1.0 g /L).

Different from degradation of phenolic compounds, only dual-reaction centres took effect on Rh B degradation because σ-Cu-ligand could not be formed between Rh B and γ-Cu-Al_2O_3-$Bi_{12}O_{15}Cl_6$. Thus, due to the highest polarization difference, γ-Cu-Al_2O_3-$Bi_{12}O_{15}Cl_6$(2.64CAB) with the strongest dual-reaction centres achieves the highest degradation rate of Rh B (Fig.3C).

To confirm the inference mentioned above, XPS spectra of catalysts before and after catalytic reaction are analyzed (Fig. S7). As for γ-Cu-Al_2O_3, the value of surface element ratio [Cu(II)/Cu(I)] increased from 1 to 1.3 and 2.06 after catalytic degradation of BPA and Rh B, respectively. Such difference can be explained as follows: (1) The chelated Cu(II) in σ-Cu-ligand was reduced to Cu(I) due to reaction of the ligands and HO-adduct radicals at the initial period of BPA degradation. On the other hand, although the chelated Cu(II) in σ-Cu(II) complex was reduced to Cu(I) during the initial period of BPA degradation, the catalytic degradation of non-phenolic compounds followed the classic Fenton reaction mechanism with the decrease of BPA. Thus, the value of surface element ratio [Cu(II)/Cu(I)] still increased slightly after catalytic degradation of BPA; (2) Without σ-Cu-ligand, most of Cu(I) was directly oxidized to Cu (II) by H_2O_2 with the generation of •OH during Rh B degradation process. Thus, more Cu (I) was oxidized to Cu (II) in degradation of Rh B than that in degradation of BPA.

Similar to γ-Cu-Al_2O_3, the value of Cu(II)/Cu(I) of γ-Cu-Al_2O_3-$Bi_{12}O_{15}Cl_6$ (0.64 CAB) increased from 1.2 to 1.48 after degradation of BPA. However, after degradation of Rh B, the Cu(II)/Cu(I) increasement of γ-Cu-Al_2O_3-$Bi_{12}O_{15}Cl_6$ (0.64 CAB) (from 1.2 to 1.4) was much lower than that of γ-Cu-Al_2O_3 (from 1.0 to 2.06). This was because most of H_2O_2 was accumulated around the electron-rich Bi centre of γ-Cu-Al_2O_3-$Bi_{12}O_{15}Cl_6$(0.64 CAB) with the generation of ·OH, resulting in decrease of the Cu(I) oxidation. With the strongest dual-reaction centres, the value of Cu(II)/Cu(I) of γ-Cu-Al_2O_3-$Bi_{12}O_{15}Cl_6$(2.64CAB) almost kept stable after catalytic degradation of BPA and Rh B. The electro-poor Cu centre could capture the electron from organics and subsequently transfer them to electro-rich Bi centre for reduction of H_2O_2 to ·OH.

In addition, the influence of H_2O_2 concentration on BPA degradation is also tested (Fig. 4C). Although the highest removal rate of TOC was achieved with the H_2O_2 concentration of 8 mM (Fig. 4D), the degradation rate of BPA did not change obviously as the H_2O_2 concentration decreased from 10 mM to 6 mM. Excess of H_2O_2 could react with OH·, which inhibited the mineralization of BPA. Thus, the H_2O_2 concentration of 8 mM was applied in the subsequent experiment for evaluation of catalyst durability (Fig. S9). As expect, even after 5 successive cycles, γ-Cu-Al_2O_3-$Bi_{12}O_{15}Cl_6$(0.64CAB and 2.64CAB) still remained high catalytic degradation rate of BPA and Rh B, respectively. Another advantage of γ-Cu-Al_2O_3-$Bi_{12}O_{15}Cl_6$(0.64CAB) is that it can be used to degrade organics in a wide range of pH. More than 97% of BPA can be degraded within 40 min in the range of pH 5–9 (Fig. S8 A). Moreover, the cotton-like morphology of γ-Cu-Al_2O_3-$Bi_{12}O_{15}Cl_6$ did not changed after the reaction, suggesting a perfect stable characterization. Bi and Al were not detected in γ-Cu-Al_2O_3-$Bi_{12}O_{15}Cl_6$ suspension. Although the slight release of Cu was detected, the concentration

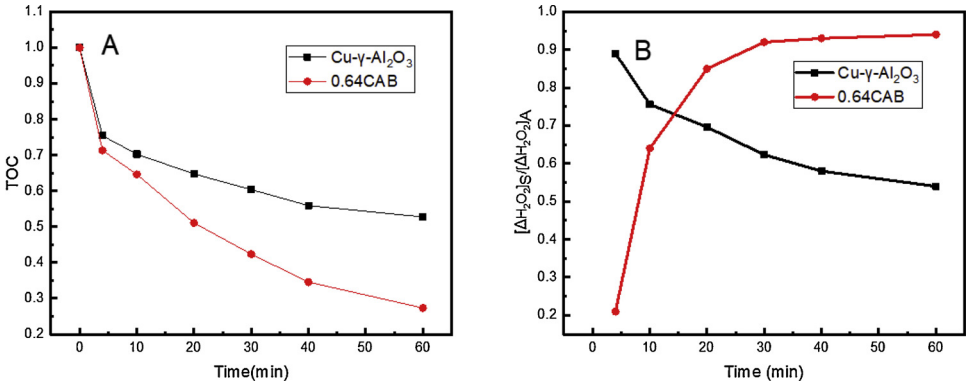

Fig. 5. (A) TOC removal of BPA over γ-Cu-Al_2O_3 and γ-Cu-Al_2O_3-$Bi_{12}O_{15}Cl_6$(0.64CAB); (B) the utilization efficiency of H_2O_2 for degradation of BPA over γ-Cu − Al_2O_3 and γ-Cu-Al_2O_3-$Bi_{12}O_{15}Cl_6$ (0.64CAB). (Initial pH = 7, initial H_2O_2 concentration = 8 mM, catalyst concentration = 1.0 g L^{-1}, initial BPA concentration = 20 mg/L).

(0.368 mg L^{-1}) was much lower than the limitation in EU directives (< 2 mg L − 1) and USA regulations (< 1.3 mg L − 1) (Fig. S8C). Our previous study also demonstrated that such low concentration Cu could not influence the heterogeneous catalytic reactions [5].

To evaluate the select conversion H_2O_2 to ·OH, TOC removal of BPA over γ-Cu-Al_2O_3 and γ-Cu-Al_2O_3-$Bi_{12}O_{15}Cl_6$ (0.64CAB) is comparatively studied. Within 90 min, γ-Cu-Al_2O_3-$Bi_{12}O_{15}Cl_6$(0.64CAB) removes 76.4% of TOC, which is much higher than γ-Cu-Al_2O_3(Fig. 5A). The utilization efficiency of H_2O_2 (η) is defined as the ratio of the stoichiometric H_2O_2 consumption ($[\Delta H_2O_2]_S$) to the actual H_2O_2 consumption ($[\Delta H_2O_2]_A$)(ABTS method showed in Supplementary material) [37]. Interestingly, η show different variation trends in γ-Cu-Al_2O_3 and γ-Cu-Al_2O_3-$Bi_{12}O_{15}Cl_6$ (0.64CAB) suspensions with the reaction time (Fig. 5B). At the beginning of degradation process, there was plenty of BPA in γ-Cu-Al_2O_3 suspensions, which could provide enough σ-Cu-ligand for select conversion H_2O_2 to ·OH. Thus, γ-Cu-Al_2O_3 showed a high value of η at the beginning of BPA degradation. However, as the reaction proceeded, BPA was degraded into intermediates (non-phenolic substance) which could not form σ-Cu-ligand with γ-Cu-Al_2O_3. Thus, generation of ·OH had to follow the classic Fenton reaction route, resulting in a low utilization of H_2O_2.

As for γ-Cu-Al_2O_3-$Bi_{12}O_{15}Cl_6$(0.64CAB), BPA preferred to be adsorbed on electron-poor Cu with the formation of σ-Cu-ligand. On one hand, σ-Cu-ligand could react with H_2O_2 for generation of ·OH and HO-adduct radicals. Such HO-adduct radicals could reduce Cu(II) to Cu(I) subsequently. On the other hand, electron-rich Bi center could also reduce H_2O_2 to ·OH, resulting in increase of ·OH production at the initial BPA degradation. Since the kinetics of BPA mineralization was much slower than that of ·OH generation, the value of η was relatively low at the initial reaction period. However, both σ-Cu-ligand and its degradation intermediates were easily mineralized by ·OH, therefore TOC removal was significantly improved in the subsequent reaction. Notably, although the σ-Cu-ligand effect gradually decreased with the decrease of phenolic compounds, both electron-rich Bi centre and OVs could still reduce H_2O_2 to ·OH for organics mineralization. Thus, γ-Cu-Al_2O_3-$Bi_{12}O_{15}Cl_6$(0.64CAB) kept high utilization efficiency of H_2O_2 (η) with the reaction time.

3.3. Catalytic mechanism

FT-IR spectra of γ-Cu-Al_2O_3-$Bi_{12}O_{15}Cl_6$ (0.64CAB) at different reaction time are used to analyze the surface reaction process (Fig. 6). Two absorption bands at 3500.9 and 1643 cm^{-1} of fresh γ-Cu-Al_2O_3-$Bi_{12}O_{15}Cl_6$(0.64CAB) are corresponded to stretching vibration of OH [ν (OH)] and blending vibration of H−O−H, respectively [38]. Characteristic peaks of −OH and $-CH_3$ of BPA appear at 3339.7 and 2970 cm^{-1}, respectively [39]. And the peaks at 1446.8, 1510, and 1610 cm^{-1} are ascribed to the skeletal vibrations of BPA aromatic rings [38,40], while the bands in the range of 1177 to 1238 cm^{-1} represented the C − O stretching vibrations of the phenolic hydroxyl

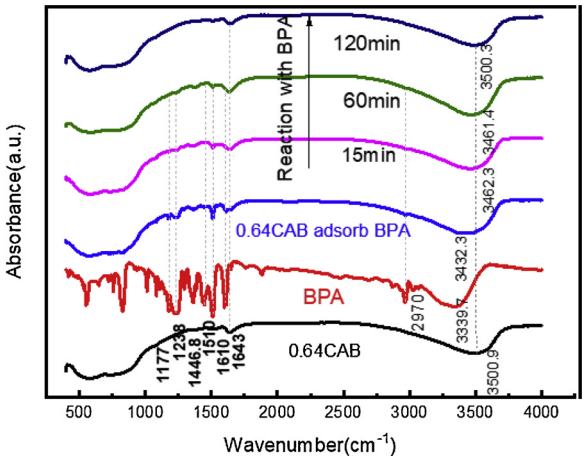

Fig. 6. FTIR spectra of various catalysts before and after reaction (Initial pH 7, initial BPA concentration 20 mg/L, initial H_2O_2 concentration 8 mM, catalyst concentration 1.0 g/L).

group [40,41]. After adsorption of BPA, the phenolic hydroxyl group of BPA could form the first coordination sphere with Cu(II) [38]. Due to the deprotonation of the phenolic hydroxyl group of BPA and the difference in surrounding, the characteristic peak of −OH shifts from 3339.7 cm^{-1} to 3423 cm^{-1}. Furthermore, some characteristic peaks of BPA also appeared in the spectra of γ-Cu-Al_2O_3-$Bi_{12}O_{15}Cl_6$(0.64CAB) after adsorption of BPA. With increase of reaction time, the characteristic peaks (1446.8, 1510, and 1610 cm^{-1}) of aromatic ring of BPA gradually disappeared. After reaction for 12 h, characteristic peaks of all organic compounds disappeared and the ν (OH) band of γ-Cu-Al_2O_3-$Bi_{12}O_{15}Cl_6$ (0.64CAB) shifted back to 3500.3 cm^{-1}, which indicated that BPA and its intermediates were mineralized completely.

In situ Raman spectra of suspension [γ-Cu-Al_2O_3-$Bi_{12}O_{15}Cl_6$(0.64CAB) + H_2O_2] in the absence and presence of BPA at different reaction time are shown in Fig. 7, which demonstrate a different catalytic mechanism from traditional electron-rich Cu centre catalysts. Since Cu(II) can combine with H_2O_2 to form transient complexes which exhibited an absorption band near 850–900 cm^{-1} [42], the signals appeared at 890 cm^{-1} are ascribed to the O − O stretching of peroxo complexes (Fig. 7A). Due to the decomposition of H_2O_2, the intensity of this peak decreased with the reaction time, and even disappeared after 10 min. Almost all the traditional Cu-based catalysts with dual-active centers provided the electron-rich Cu centre for reduction of H_2O_2 to OH. However, as for the suspension of γ-Cu-Al_2O_3-$Bi_{12}O_{15}Cl_6$, H_2O_2 will be oxidized to O_2 by eletron-poor Cu centre in the absence of organics. Thus, it is observed that large amount of bubbles (O_2) escaped from liquid (Fig. 7C) without addition of BPA. Meanwhile, the generation of O_2 increased with the Bi content due to higher polarization differences of γ-Cu-Al_2O_3-$Bi_{12}O_{15}Cl_6$. On the contrary, the

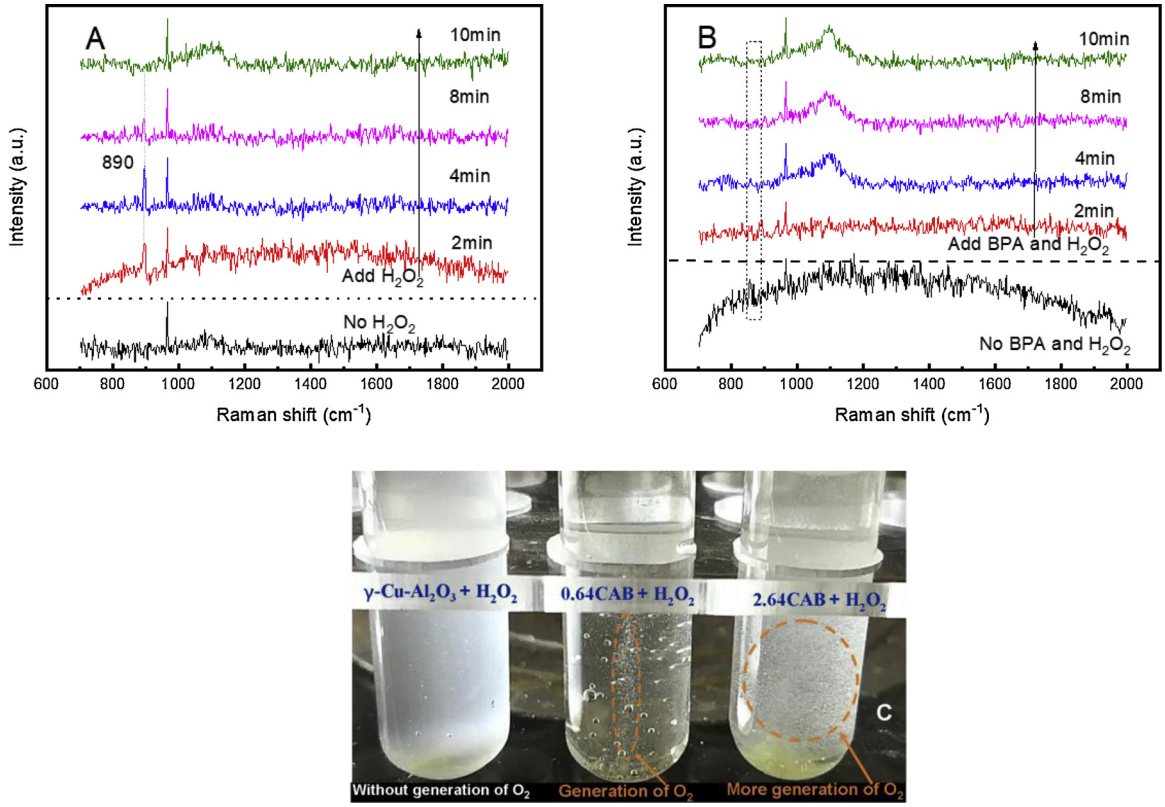

Fig. 7. In situ Raman spectra for 0.64CAB aqueous dispersions at different time: (A) 0.64CAB reacting with H_2O_2; (B) 0.64CAB reacting with BPA and H_2O_2. (C) Photos of O_2 generation in different suspensions.

O − O stretching vibration band disappeared as BPA is added in (Fig. 7B), which indicates that the peroxo complexes are not formed in the suspension of (γ-Cu-Al_2O_3-$Bi_{12}O_{15}Cl_6$ + H_2O_2 + BPA). Compared with H_2O_2, BPA was preferentially adsorbed on electron-poor Cu centre of γ-Cu-Al_2O_3-$Bi_{12}O_{15}Cl_6$ with the formation of σ-Cu-ligand.

To further elucidate the catalytic mechanism, DMPO-trapped EPR signals are detected in different dispersions of the corresponding samples (Fig. 8). In the absence of H_2O_2, no signals are detected in the methanol dispersion of pure Al_2O_3 and $Bi_{12}O_{15}Cl_6$ (Fig. 8A). However, six characteristic peaks of DMPO–$O_2^{\cdot-}$ are observed with the intensities following the order of γ-Cu-Al_2O_3 > γ-Cu-Al_2O_3-$Bi_{12}O_{15}Cl_6$(0.64CAB) > γ-Cu-Al_2O_3-$Bi_{12}O_{15}Cl_6$(2.64CAB). The other peaks are assigned to the carbon centre radicals generated from the reaction between DMPO and $O_2^{\cdot-}$ [43]. Since these peaks overlapped with the characteristic peaks of DMPO –O_2^{-}, it was difficult to identified them from the EPR spectra. Our previous study had already demonstrated that the O_2^{-} could be generated from the reaction of the electron-rich centre and O_2 [5]. Thus, in the methanol dispersion of γ-Cu-Al_2O_3-$Bi_{12}O_{15}Cl_6$, $Bi_{12}O_{15}Cl_6$ could act as the electron-rich centre for reduction of O_2 to O_2^{-}. However, the generation of O_2^{-} over γ-Cu-Al_2O_3-$Bi_{12}O_{15}Cl_6$(0.64CAB) was higher than that over γ-Cu-Al_2O_3-$Bi_{12}O_{15}Cl_6$(2.64CAB), which did not correspond to their polarity difference of dual-reaction centres. Such phenomenon could be explained as follows. The OVs on the surface of γ-Cu-Al_2O_3-$Bi_{12}O_{15}Cl_6$ increased with the $Bi_{12}O_{15}Cl_6$ content. OVs can be easily healed by O_2 [44], which decreased the reduction of O_2 to $O_2^{\cdot-}$ over electron-rich Bi centre. Thus, the highest generation of $O_2^{\cdot-}$ was observed over γ-Cu-Al_2O_3-$Bi_{12}O_{15}Cl_6$(0.64CAB).

Due to the oxidation of H_2O to ·OH by electron-poor Cu centre, characteristic peaks (marked with ●) of DMPO − $OH^{\cdot}$ are observed in γ-Cu-Al_2O_3 aqueous solution and γ-Cu-Al_2O_3-$Bi_{12}O_{15}Cl_6$ aqueous solution (Fig. 8B). Their intensities followed the order of γ-Cu-Al_2O_3-$Bi_{12}O_{15}Cl_6$(2.64CAB) > γ-Cu-Al_2O_3-$Bi_{12}O_{15}Cl_6$(0.64CAB) > γ-Cu-Al_2O_3, which was consistent to their polarity differences. In addition, $^{\cdot}$OH attacked carbon-containing compounds (DMPO) with the production of carbon-centred radical adduct [45], appearing as the other six peaks (marked with ◆). Furthermore, the intensity of characteristic peak (DMPO − $OH^{\cdot}$) in γ-Cu-Al_2O_3-$Bi_{12}O_{15}Cl_6$(0.64CAB) suspensions with H_2O_2 is obviously increased after addition of BPA (Fig. 8C), suggesting that σ-Cu-ligand can significantly enhance the conversion H_2O_2 to $OH^{\cdot}$. BPA is preferentially adsorbed onto the electron-poor Cu centre with the formation of σ-Cu-ligand. Such σ-Cu-ligand could be oxidized to HO-adduct radicals with the generation of $^{\cdot}$OH. Thus, addition of BPA obviously increased the intensity of DMPO − OH in γ-Cu-Al_2O_3-$Bi_{12}O_{15}Cl_6$(0.64CAB) suspensions with H_2O_2.

Moreover, the intensity of DMPO − OH· almost keep stable during the whole reaction process in the suspension of γ-Cu-Al_2O_3-$Bi_{12}O_{15}Cl_6$(0.64CAB) and H_2O_2 (Fig. 8D), which demonstrates that dual-reaction centres of γ-Cu-Al_2O_3-$Bi_{12}O_{15}Cl_6$(0.64CAB) still play important role in generation of OH without σ-Cu-ligand. Thus, in the suspension of [γ-Cu-Al_2O_3-$Bi_{12}O_{15}Cl_6$(0.64CAB) + H_2O_2 + BPA], the highest intensity of DMPO − OHis achieved at the initial 0–4 min due to the synergistic effect of σ-Cu-ligand and dual-reaction centers (Fig. 8E). After reaction for 10 min, ·OH generated from the reaction of σ-Cu-ligand and H_2O_2 decreased obviously because most phenolic compounds were degraded into non-phenolic compounds. Thus, dual-reaction centers gradually played dominant role in generation of ·OH, resulting in a stable intensity of DMPO − OH. Different from γ-Cu-Al_2O_3-$Bi_{12}O_{15}Cl_6$(0.64CAB), the generation of ·OH in the suspension of (γ-Cu-Al_2O_3 + H_2O_2 + BPA) was relied on the reaction of σ-Cu-ligand and H_2O_2, which leaded to a decline of DMPO − OH· intensity with the time (Fig.8F).

In addition, the intensities of DMPO–$O_2^{\cdot-}$ follow the order of γ-Cu-Al_2O_3 > 0.64CAB > 2.64CAB in the presence of H_2O_2 and BPA (Fig. 8G). Since $O_2^{\cdot-}$ was generated from Eq. (2), the intensity of DMPO–$O_2^{\cdot-}$ is inversely to selective conversion H_2O_2 to ·OH. Being

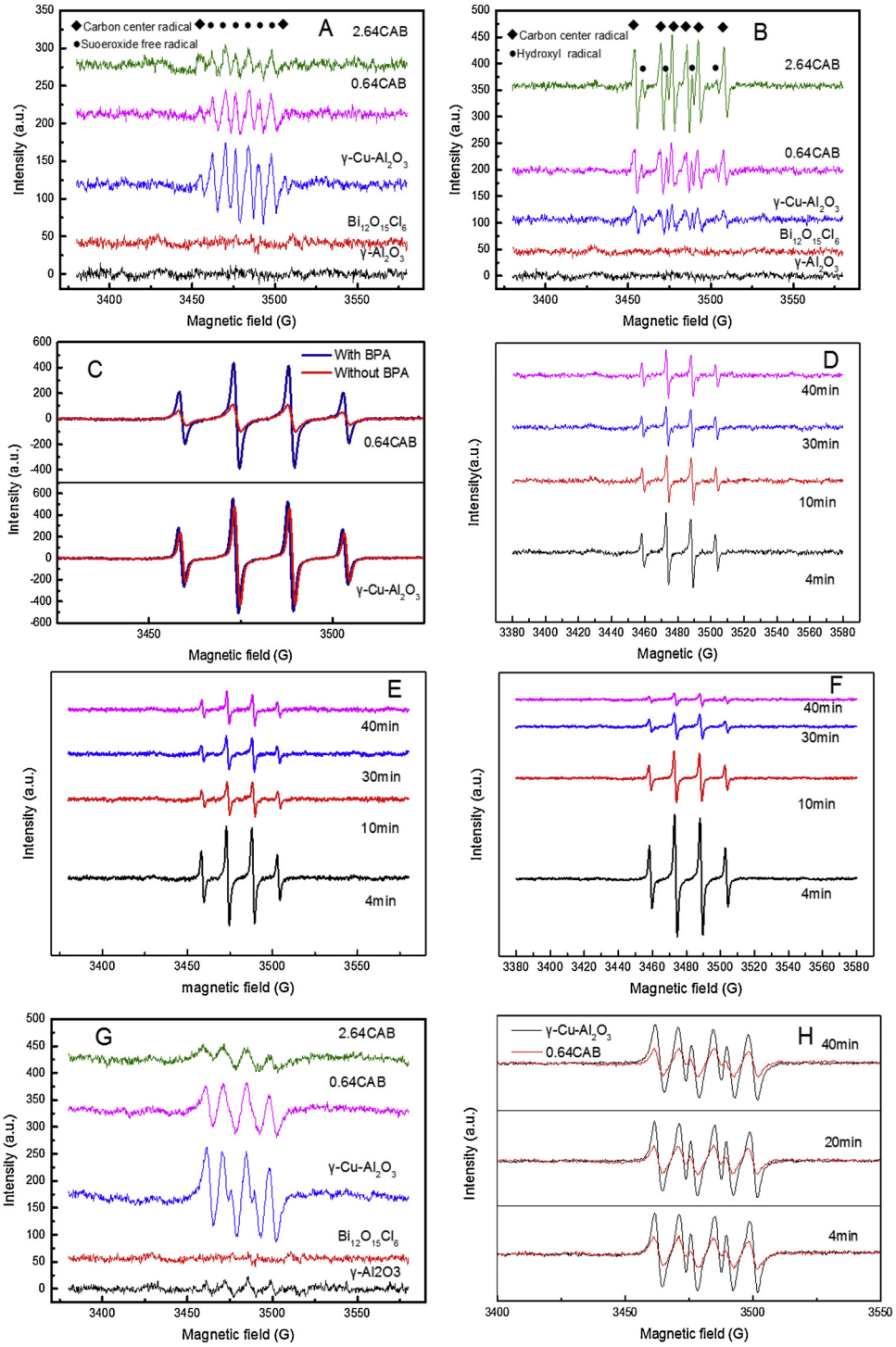

Fig. 8. DMPO spin-trapping EPR spectra for (A) HO_2/O_2^- in various methanol dispersions and (B) OH in various methanol dispersions without H_2O_2. (C)·OH in γ-Cu-Al_2O_3-$Bi_{12}O_{15}Cl_6$(0.64CAB) suspensions with H_2O_2 in the present and absent of BPA (D) OH in 0.64 CAB aqueous suspensions with H_2O_2 at different time. (E) OH in 0.64 CAB aqueous suspensions with H_2O_2 and BPA at different time. (F) ·OH in γ-Cu-Al_2O_3 aqueous suspensions with H_2O_2 and BPA at different time. (G) HO_2/O_2^- in various methanol dispersions in the presence of H_2O_2 and BPA. (H) $HO_2\cdot/O_2\cdot^-$ in γ-Cu-Al_2O_3 and 0.64 CAB methanol dispersions with H_2O_2 and BPA at different time.

attributed to the highest polarity difference, γ-Cu-Al_2O_3-$Bi_{12}O_{15}Cl_6$(2.64CAB) possessed the strongest dual-reaction centres, resulting in the highest selective conversion H_2O_2 to OH. Although DMPO–O_2·- is detected in the dispersion of [γ-Cu-Al_2O_3-$Bi_{12}O_{15}Cl_6$(2.64CAB) + H_2O_2 + BPA] (Fig.8H), its intensity is much lower than that in dispersion of [γ-Cu-Al_2O_3 + H_2O_2 + BPA] during the whole reaction process. Thus, γ-Cu-Al_2O_3-$Bi_{12}O_{15}Cl_6$(2.64CAB) achieved the higher selective conversion H_2O_2 to OH.

On the other hand, large amounts of OVs are formed in $Bi_{12}O_{15}Cl_6$ during the calcining process (BiOCl→$Bi_{12}O_{15}Cl_6$) (Fig. 9A, B), which can also increase the generation of OH (OV + H_2O_2→•OH + OH^-) [46]. The characteristic peaks of DMPO−OH· are detected in the suspension of $Bi_{12}O_{15}Cl_6$ and H_2O_2 but not in the suspension of BiOCl and H_2O_2 (Fig.9D), which confirm the reduction of H_2O_2 to ·OH by OVs of $Bi_{12}O_{15}Cl_6$. Thus, $Bi_{12}O_{15}Cl_6$ show higher removal rate of Rh B than BiOCl within 40 min (Fig. 9C). In addition, the characteristic peaks of O 1 s in Fig. S5(B) indicates that the surface O 1 s peak area takes high proportion of total O 1 s peak area, which confirms the existence of large amounts of OVs in γ-Cu-Al_2O_3-$Bi_{12}O_{15}Cl_6$(0.64CAB) [14,47]. Since the localized electrons on OVs can be transferred to Bi^{3+} with the generation of lower charge Bi ions ($Bi^{(3-x)+}$), new peaks with lower binding energy (157.3 eV, 162.7 eV) appear in the spectra of Bi 4f of γ-Cu-Al_2O_3-$Bi_{12}O_{15}Cl_6$(0.64CAB) [28,29]. Thus, these two side characteristic peaks of Bi $4f_{7/2}$ and Bi $4f_{5/2}$ further confirmed the existence

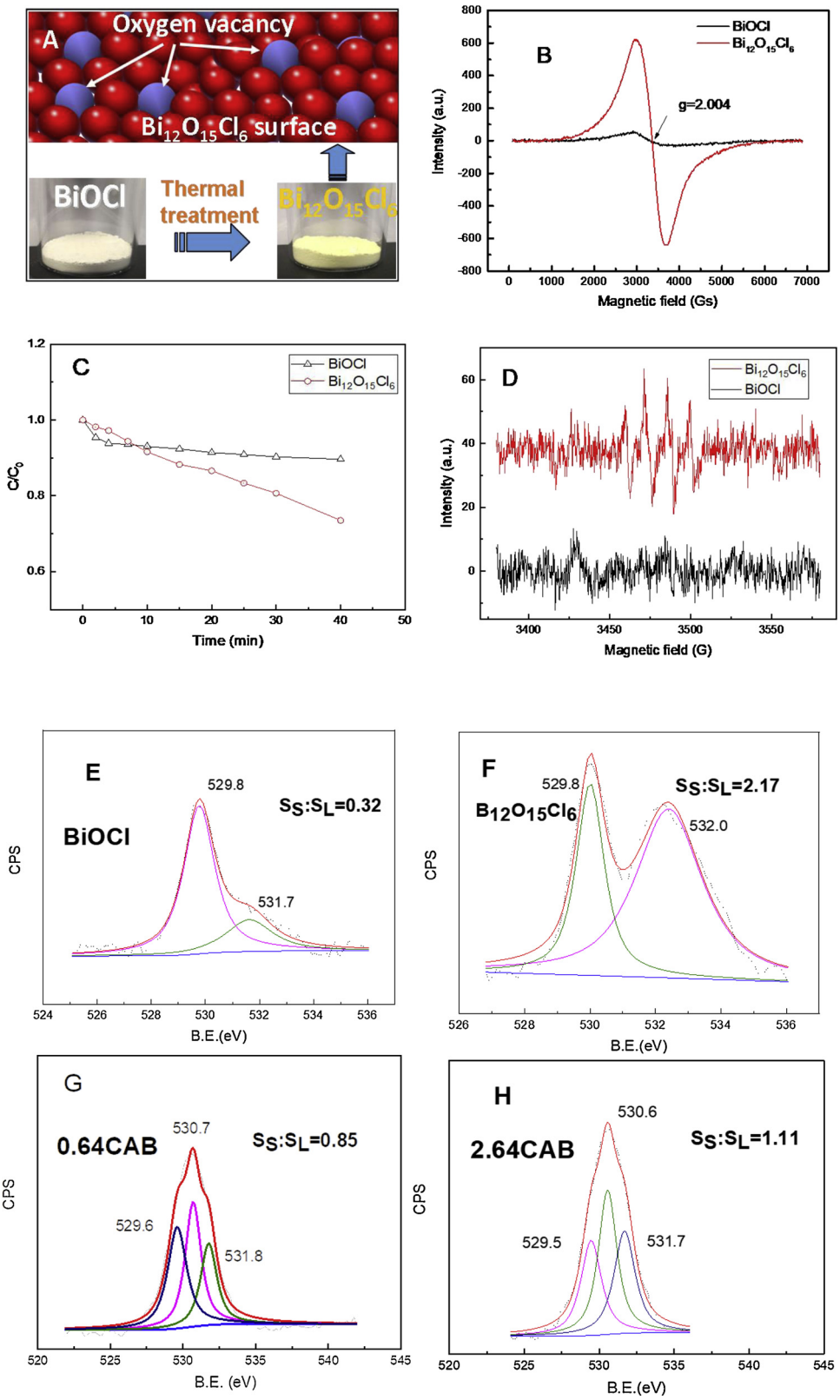

Fig. 9. (A) Schematic formation of surface OVs on $Bi_{12}O_{15}Cl_6$. (B) Solid EPR spectra of BiOCl and $Bi_{12}O_{15}Cl_6$. (C) Degradation of Rh B over BiOCl and $Bi_{12}O_{15}Cl_6$, (D) DMPO spin-trapping EPR spectra for $^{\cdot}OH$ in BiOCl and $Bi_{12}O_{15}Cl_6$ aqueous suspensions with H_2O_2 and Rh B. The ratio of the surface O 1 s peaks area to the lattice O 1 s peaks area to ($R = S_S/S_L$) (E) BiOCl (R = 0.32) (F) $Bi_{12}O_{15}Cl_6$(R = 2.17) (G) γ-Cu-Al_2O_3-$Bi_{12}O_{15}Cl_6$ (0.64CAB) (R = 0.85) (H) γ-Cu-Al_2O_3-$Bi_{12}O_{15}Cl_6$ (2.64CAB) (R = 1.11).

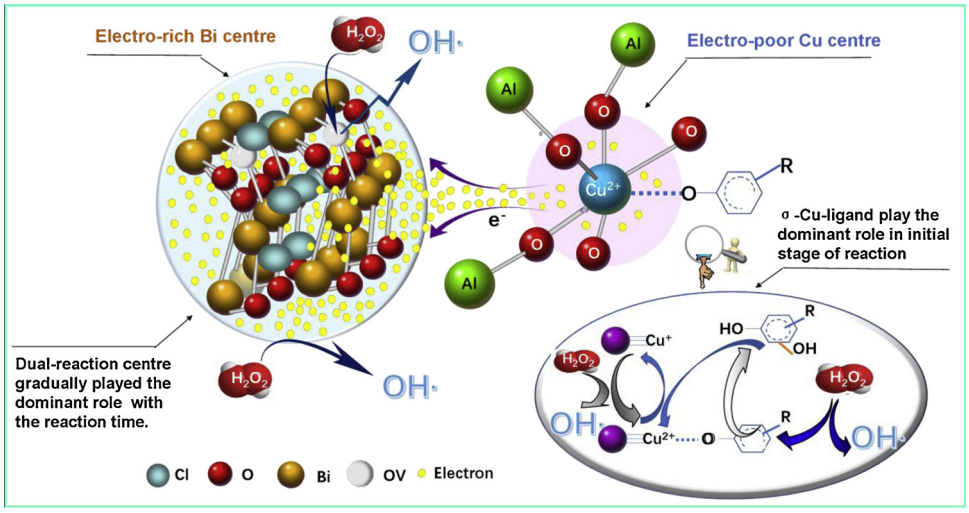

Fig. 10. The catalytic degradation mechanism of phenolic compounds over γ-Cu-Al_2O_3-$Bi_{12}O_{15}Cl_6$ (0.64CAB).

of large amounts of OVs in the $Bi_{12}O_{15}Cl_6$ of γ-Cu-Al_2O_3-$Bi_{12}O_{15}Cl_6$.

Furthermore, the proportion of OVs in γ-Cu-Al_2O_3-$Bi_{12}O_{15}Cl_6$ can be calculated according to the ratio of the surface O 1 s peak area to the lattice O 1 s peak area ($R = S_S/S_L$) [14,47]. The higher value of R indicates the larger amount of OVs on the catalyst surface. The proportion of OVs ($R = S_S/S_L$) on different catalysts surface followed the order of pure BiOCl (R = 0.32) < γ-Cu-Al_2O_3-$Bi_{12}O_{15}Cl_6$ (0.64CAB) (R = 0.85) < γ-Cu-Al_2O_3-$Bi_{12}O_{15}Cl_6$ (2.64CAB) (R = 1.11) < pure $Bi_{12}O_{15}Cl_6$(R = 2.17) (Fig. 9 E–H). Thus, the amount of OVs in γ-Cu-Al_2O_3-$Bi_{12}O_{15}Cl_6$ is increased with the $Bi_{12}O_{15}Cl_6$ content, which can clearly demonstrate that OVs in γ-Cu-Al_2O_3-$Bi_{12}O_{15}Cl_6$ catalyst still exist in $Bi_{12}O_{15}Cl_6$. Notably, although two side peaks of Bi $4f_{7/2}$ and Bi $4f_{5/2}$ disappear after reaction due to the exhaustion of OVs, the main characteristic peak of Bi does not shift obviously (Fig. S10C). Thus, the existence of OVs did not affect the electron clound density of Bi obviously. In order to better analyze the influence of OVs on electron density of Cu, the solid EPR of Cu of γ-Cu-Al_2O_3-$Bi_{12}O_{15}Cl_6$ (2.64CAB) before and after reaction were conducted. As shown in Fig. S10(D), the EPR characteristic peak of Cu does not change obviously after reaction, which also indicates that the existence of OVs did not change the electron clound of Cu obviously.

However, the value of S_s/S_L of γ-Cu-Al_2O_3-$Bi_{12}O_{15}Cl_6$(0.64CAB) decreases from 0.85 to 0.1 (Fig. 9G and Fig. S10 A) after reaction, which indicates that the OVs in γ-Cu-Al_2O_3-$Bi_{12}O_{15}Cl_6$ were almost exhausted. By calcination, the OVs on γ-Cu-Al_2O_3-$Bi_{12}O_{15}Cl_6$(0.64CAB) can be well regenerated (Fig. S10 B). On the other hand, although the OVs contributed to the catalytic activity, it did not play the dominant role in catalytic reaction process. The synergistic effect of dual-reaction centres and σ-Cu-ligand played the dominant role in catalytic degradation process of phenolic compounds.

Based on the above results, the possible catalytic mechanism is proposed (Fig. 10), which is different from traditional electron-rich Cu centre catalysts. In the system of [γ-Cu-Al_2O_3-$Bi_{12}O_{15}Cl_6$ (0.64CAB) + H_2O_2 + phenolic compounds], the electron-poor Cu centre could facilitate the formation of σ-Cu-ligand with phenolic compounds. Such σ-Cu-ligand were preferentially oxidized by H_2O_2 with the generation of ·OH and HO-adduct radicals, and the HO-adduct radicals reduced Cu(II) to Cu(I) subsequently. Thus, the σ-Cu-ligand not only prevented Cu(II) from oxidizing H_2O_2 to $HO_2^{\cdot}/O_2^{\cdot-}$ but also enhanced the redox cycle of Cu(II)/Cu(I). Notably, although the σ-Cu-ligand was gradually decreased with the time due to the degradation of phenolic compounds, dual-reaction centres could still play the important role in catalytic reaction. Both electron-rich Bi center and OVs could reduce H_2O_2 to OH for organics degradation. Thus, ·OH could be generated by four electron transfer routes during the degradation process of phenolic compunds: (1) the first transfer route was from σ-Cu-ligand to H_2O_2, with the generation of OH and reduction of Cu(II) to Cu(I); (2) the second transfer route was from Cu(I) to H_2O_2 with the generation of OH; (3) the third transfer route was from electron-rich Bi centre to H_2O_2 with the generation of OH; and (4) the fourth transfer route was from OVs to H_2O_2 with the generation of ·OH. Being attributed to the synergistic effect of σ-Cu-ligand, dual-reaction centre and OVs mentioned above, γ-Cu-Al_2O_3-$Bi_{12}O_{15}Cl_6$ achieved high catalytic activity and utilization efficiency of H_2O_2 (η).

4. Conclusion

Novel Fenton-like catalyst γ-Cu-Al_2O_3-$Bi_{12}O_{15}Cl_6$ with electron-poor Cu centre and electron-rich Bi centre was constructed for selective degradation of phenolic compounds. Different from traditional electro-rich Cu centre catalysts, the electron-poor Cu centre could facilitate the formation of σ-Cu-ligand with phenolic compounds. Such σ-Cu-ligand could be oxidized to HO-adduct radicals by H_2O_2 with the generation of OH, and the Cu(II) in σ-Cu(II) complexes was simultaneously reduced to Cu(I) by HO-adduct radicals. Notably, although σ-Cu-ligand effect was gradually weakened with the reaction time due to the decrease of phenolic compounds, dual-reaction centres played the dominant role in catalytic reaction. Both electron-rich Bi center and OVs could reduce H_2O_2 to OH for non-phenolic compounds degradation. Due to the synergistic effect of σ-Cu-ligand, dual-reaction centres and OVs, γ-Cu-Al_2O_3-$Bi_{12}O_{15}Cl_6$ not only showed high degradation rate of phenolic compounds but also achieved high utilization efficiency of H_2O_2 (η).

Acknowledgement

This research was supported by National Natural Science Foundation of China (No. 51878335), Water Resource Research Project of Jiangsu Province (2017043) and Natural Science Foundation of Jiangsu province. We also acknowledge the generous support provided by the State Key Program of National Natural Science of China (No. 51438008).

Appendix A. Supplementary data

Supplementary material related to this article can be found, in the online version, at doi:https://doi.org/10.1016/j.apcatb.2019.04.032.

References

[1] L. Lyu, L. Zhang, Q. Wang, Y. Nie, C. Hu, Environ. Sci. Technol. 49 (2015)

8639–8647.
[2] R. Salazar, E. Brillas, I. Sires, Appl. Catal. B: Environ. 115 (2012) 107–116.
[3] L. Lyu, D. Yan, G. Yu, W. Cao, C. Hu, Environ. Sci. Technol. 52 (2018) 4294–4304.
[4] L. Lyu, L. Zhang, G. He, H. He, C. Hu, J. Mater. Chem. A 5 (2017) 7153–7164.
[5] S. Xu, H. Zhu, W. Cao, Z. Wen, J. Wang, C.P. François-Xavier, T. Wintgens, Appl. Catal. B: Environ. 234 (2018) 223–233.
[6] L. Lyu, L. Zhang, C. Hu, Environ. Sci. Nano 3 (2016) 1483–1492.
[7] S. Ullah, E.P. Ferreira-Neto, C. Hazra, R. Parveen, H.D. Rojas-Mantilla, M.L. Calegaro, Y.E. Serge-Correales, U.P. Rodrigues-Filho, S.J.L. Ribeiro, Appl. Catal. B: Environ. 243 (2019) 121–135.
[8] C. Liu, J. Zhou, J. Su, L. Guo, Appl. Catal. B: Environ. 241 (2019) 506–513.
[9] H. Zhang, H. Li, Z. Wang, Z. Zheng, P. Wang, Y. Liu, X. Zhang, X. Qin, Y. Dai, B. Huang, Appl. Catal. B: Environ. 238 (2018) 586–591.
[10] F. Chen, Q. Yang, F. Yao, Y. Ma, Y. Wang, X. Li, D. Wang, L. Wang, H. Yu, Chem. Eng. J. 355 (2019) 624–636.
[11] F. Chen, Q. Yang, X. Li, G. Zeng, D. Wang, C. Niu, J. Zhao, H. An, T. Xie, Y. Deng, Appl. Catal. B: Environ. 200 (2017) 330–342.
[12] F. Deng, Q. Zhang, L. Yang, X. Luo, A. Wang, S. Luo, D.D. Dionysiou, Appl. Catal. B: Environ. 238 (2018) 61–69.
[13] L. Zhang, L. Lyu, Y. Nie, C. Hu, Sep. Purif. Technol. 157 (2016) 203–208.
[14] L. Wang, D. Yan, L. Lyu, C. Hu, N. Jiang, L. Zhang, J. Colloid Interface Sci. 527 (2018) 251–259.
[15] X. Shi, P. Wang, W. Li, Y. Bai, H. Xie, Y. Zhou, L. Ye, Appl. Catal. B: Environ. 243 (2019) 322–329.
[16] Y. Zhang, C. Lin, Q. Lin, Y. Jin, Y. Wang, Z. Zhang, H. Lin, J. Long, X. Wang, Appl. Catal. B: Environ. 235 (2018) 238–245.
[17] D. Chen, J. Yang, Y. Zhu, Y. Zhang, Y. Zhu, Appl. Catal. B: Environ. 233 (2018) 202–212.
[18] J. Li, Y. Yu, L. Zhang, Nanoscale 6 (2014) 8473–8488.
[19] J. Zhong, Y. Zhao, L. Ding, H. Ji, W. Ma, C. Chen, J. Zhao, Appl. Catal. B: Environ. 241 (2019) 514–520.
[20] M. Guerrero, S. Pane, B.J. Nelson, M.D. Baro, M. Roldan, J. Sort, E. Pellicer, Nanoscale 5 (2013) 12542–12550.
[21] J. Di, J. Xia, S. Yin, H. Xu, L. Xu, Y. Xu, M. He, H. Li, RSC Adv. 4 (2014).
[22] Y. Myung, F. Wu, S. Banerjee, A. Stoica, H. Zhong, S.-S. Lee, J. Fortner, L. Yang, P. Banerjee, Chem. Mater. 27 (2015) 7710–7718.
[23] W. Gu, J. Xu, F. Teng, Z. Ul Abideen, ChemistrySelect 3 (2018) 10721–10726.
[24] H. Cai, X. Liu, J. Zou, J. Xiao, B. Yuan, F. Li, Q. Cheng, Chemosphere 193 (2018) 833–839.
[25] K.I. Shimizu, H. Kawabata, H. Maeshima, A. Satsuma, T. Hattori, J. Phys. Chem. B 104 (2000).
[26] S. Guo, D. Li, L. Zhang, J. Li, E. Wang, Biomaterials 30 (2009) 1881–1889.
[27] C.Y. Wang, X. Zhang, X.N. Song, W.K. Wang, H.Q. Yu, ACS Appl. Mater. Interfaces 8 (2016) 5320–5326.
[28] L. Ye, L. Zan, L. Tian, T. Peng, J. Zhang, Chem. Commun. (Camb.) 47 (2011) 6951–6953.
[29] L. Ye, K. Deng, F. Xu, L. Tian, T. Peng, L. Zan, Phys. Chem. Chem. Phys. 14 (2012) 82–85.
[30] R.-R. Cheng, Z.-L. Wu, Y.-L. Hou, J. Dong, J.-Z. Cui, B. Zhao, Inorg. Chem. Commun. 51 (2015) 95–98.
[31] W. Wang, Q. Zhu, F. Qin, Q. Dai, X. Wang, Chem. Eng. J. 333 (2018) 226–239.
[32] M. Zhang, H. Fan, X. Ren, N. Zhao, H. Peng, C. Wang, X. Wu, G. Dong, C. Long, W. Wang, Y. Gao, L. Ma, P. Wu, H. Li, X. Jiang, J. Power Sources 418 (2019) 202–210.
[33] G. Dong, H. Fan, K. Fu, L. Ma, S. Zhang, M. Zhang, J. Ma, W. Wang, Compos Part B-Eng 162 (2019) 369–377.
[34] C. Wang, H. Fan, X. Ren, Y. Wen, W. Wang, Appl. Surf. Sci. 462 (2018) 423–431.
[35] H. Tian, H. Fan, J. Ma, Z. Liu, L. Ma, S. Lei, J. Fang, C. Long, J. Hazard. Mater. 341 (2018) 102–111.
[36] L. Ma, H. Fan, K. Fu, S. Lei, Q. Hu, H. Huang, G. He, ACS Sustain. Chem. Eng. 5 (2017) 7093–7103.
[37] M.L. Kuznetsov, Y.N. Kozlov, D. Mandelli, A.J. Pombeiro, G.B. Shul'pin, Inorg. Chem. 50 (2011) 3996–4005.
[38] Ž. Mitić, G.S. Nikolić, M. Cakić, P. Premović, L. Ilić, J. Mol. Struct. 924-926 (2009) 264–273.
[39] Y. Mikhaylova, G. Adam, L. Häussler, K.J. Eichhorn, B. Voit, J. Mol. Struct. 788 (2006) 80–88.
[40] W. Guo, W. Hu, J. Pan, H. Zhou, W. Guan, X. Wang, J. Dai, L. Xu, Chem. Eng. J. 171 (2011) 603–611.
[41] X. Li, X. Dai, J. Takahashi, N. Li, J. Jin, L. Dai, B. Dong, Bioresour. Technol. 159 (2014) 412–420.
[42] C. Wang, L. Liu, L. Zhang, Y. Peng, F. Zhou, Biochemistry 49 (2010) 8134–8142.
[43] L. Wang, F. Wang, P. Li, L. Zhang, Sep. Purif. Technol. 120 (2013) 148–155.
[44] K. Onda, B. Li, H. Petek, Phys. Rev., B Condens. Matter (2004) 70.
[45] L. Khachatryan, B. Dellinger, Environ. Sci. Technol. 45 (2011) 9232–9239.
[46] H. Li, J. Shang, Z. Yang, W. Shen, Z. Ai, L. Zhang, Environ. Sci. Technol. 51 (2017) 5685–5694.
[47] W. Cao, O.K. Tan, J.S. Pan, W. Zhu, C.V.G.J.M.C. Reddy, Physics 75 (2002) 67–70.